EARTHQUAKE ENGINEERING AND STRUCTURAL DYNAMICS, VOL. 25, 671–688 (1996)

# BEAM GLOBAL MODEL FOR THE SEISMIC ANALYSIS OF RC FRAMES

D. MIRAMONTES*, O. MERABET AND J. M. REYNOUARD

*Laboratoire Bétons et Structures, INSA-Lyon (National Institute of Applied Sciences at Lyon), 20, Av.A. Einstein, Bât. 304, 69621 Villeurbanne, France*

## SUMMARY

A new hysteretic beam model based on a moment–curvature uniaxial cyclic law is proposed. The model is characterized by a trilinear envelope curve and a set of cyclic rules. The strength and stiffness degradation in the hardening and the softening branches as well as the hysteretic damping are directly dependent on the level and history of loading. Their continuous evolution is described with the aid of a new parameter based on energy criteria and phenomenological considerations. The model is capable of describing the dynamic response of RC frames with a minimum of input parameters.

The characteristic points of the envelope curve are defined by three critical strain conditions at cross-section level. A revision of ultimate compressive strain of concrete is used to start the softening behaviour of the envelope curve. The principal phenomena taken into account by the hysteretic rules are: stiffness degradation and strength reduction due to cyclic loading, pinching of loops due to shear stress, softening behaviour at failure and the effect of axial force due to gravity loads. The evolution of cyclic behaviour is controlled by a new cyclic parameter defined in terms of a damage index, an accommodation factor and the number of cycles with amplitude inferior to the maximum strain (curvature) ever experienced. This parameter allows the description of monotonic and cyclic response for both small and large deformations, including the post-peak regime.

In order to validate the proposed model, the global response of isolated members as well as a complete structure subjected to cyclic and dynamic loads are compared with experiments.

KEY WORDS: RC frame; hysteretic model; generalized variables; cyclic parameter; energy dissipation; degradation process

## 1. INTRODUCTION

A good representation of the hysteretic behaviour of reinforced concrete structures depends strongly on the modelling of material non-linearities and structural damage throughout a cyclic loading scenario. However, the non-linear analysis of structures subjected to dynamic loads represents a high constraint due to the volume of non-linear calculations needed to integrate the equilibrium equations for each time-step, and consequently a precise choice between the computational time and the scale description arises.

The study of the damage process and the vulnerability to collapse of RC structures under earthquake loading requires the formulation of numerical models capable of describing the non-linear behaviour of structural members (beams, columns, slabs, etc.). Taking into account the diversity and complexity of structures, a brief description of different modelling scales includes (Figure 1):

(1) Local models,[1] which use a continuous media approach and the constitutive law expressed in local variables is independent of geometry. All parameters have a physical meaning and are taken from standard tests. The finite element method requires the solution of a large system of equations, the calculation of behaviour law in numerous internal points and the integration of stress in two or three space directions.
(2) Global models,[2] which are formulated in generalized variables that take into account the concrete and steel properties. The integration of stress at cross-section level is eliminated and the number of points

*Also at Escuela de Ingenieria, Universidad Autonoma de Zacatecas, Av. Lopez V. No 801, 98000 Zacatecas, Zac., México

CCC 0098–8847/96/070671–18

*Received 14 October 1995*
*Revised 23 January 1996*

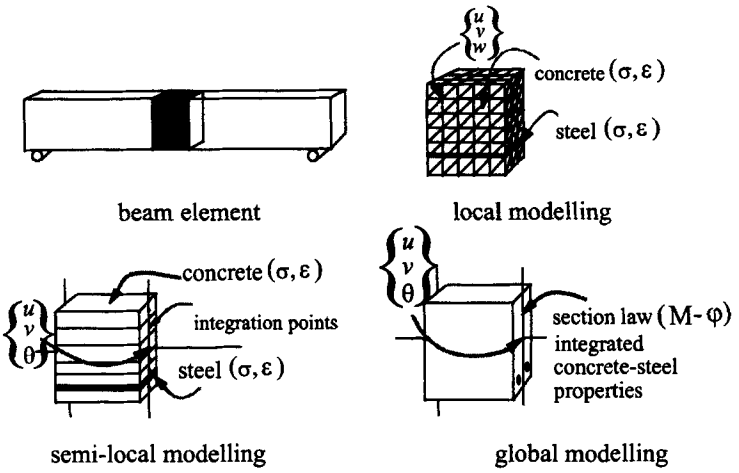


Figure 1. Three modelling scales

defining the behaviour law is reduced (trilinear or even bilinear behaviour laws). These models are formulated considering simplified kinematic hypothesis (Navier–Bernoulli or Timoshenko for beams, Kirchhoff–Love or Reissner–Mindlin for shells). The concrete-steel behaviour is described in generalized variables as uniaxial behaviour laws based on experimental observations $(N, \varepsilon)$, $(V, \gamma)$, $(M, \phi)$ or based on classical theories of plasticity or damage mechanical models (i.e. yielding surface $f(N, V, M) = 0)$) . The loss of local information represents the principal drawback of these models. Furthermore they should be specialized for each cross-section and particular loading histories (earthquakes, impacts, explosions, etc.). Indeed, the reduced CPU time required and the adequate simulation of global hysteretic behaviour make these models an attractive tool-kit for sequentially non-linear dynamic analysis of complete structures.

(3) Semi-local models,[3] which stand between a local and a global formulation, using some global model hypotheses (2-D multilayered beams/plates/shells models and 3-D multifibre beam models). The equilibrium and kinematic conditions are managed at global scale whereas stress and internal variables are calculated at local level. This intermediate scale allows exploitation of the simplified kinematic hypothesis of the theory of beams with a consequent reduction of the size of the equation system, and on the other hand, permits a fast integration of the behaviour laws thanks to the uniaxial hypothesis of the strain–stress field.

A combination of the preceding formulations leads to the adaptive models,[4] for which the main components are: the elastic formulation, the elasto-plastic formulation and the automatic mesh refinement. The analysis is started using one elastic element per member. During analysis these elements are checked for the occurrence of inelasticity, and those elastic elements which have undergone inelastic deformation are removed and replaced appropriately by new quartic elastic and cubic inelastic elements based on a layered approach. These models hold the promise of economy and accuracy.

At the local level, the implementation of complex laws enables the correct description of the observed experimental evolution in almost all the cases. However, this fine and expensive description cannot be applied systematically in the case of industrial applications which require the representation of hundreds or even thousands of degrees of freedom. Due to kinematic hypotheses, the semi-local approach reduces significantly the computational time. Nevertheless, this approach may still be considered expensive in the case of analysis of real structures under dynamic excitation such as earthquake loading.

The objective of this paper is to develop an efficient RC beam global model to simulate properly the hysteretic behaviour of a structure composed of beams and columns, that can be used during the design of structures or the elaboration of building codes.

## 2. HYSTERETIC MODEL

### 2.1. *Framework and scope*

Several global models have been proposed during the last thirty years to describe the inelastic cyclic response of structures. They can be grouped in two major categories:

(a) The phenomenological models,[2,5,6] defined by orthogonal uniaxial laws, $(N, \varepsilon)$; $(V, \gamma)$; $(M, \phi)$. Most of such earlier models neglect the occurrence of permanent strains before yielding. Hence, degradation and dissipation processes begin after the yield condition. The strength reduction is modelled by constant parameters[5] or constant reloading points[6] independent of cyclic loading. A better description is based on the accumulated hysteretic energy.[2] However, the effect of this quantity for subsequent cyclic loading for a fixed strain level should vanish in order to describe the cyclic stabilization phenomenon.

(b) The classical plasticity models[7,8] or the damage mechanical models,[9,10] defined by yield surfaces (i.e. interaction diagrams $f(N, V, M) = 0$). The inelastic interaction between bending moments, torque and axial force is considered by means of yield interaction surfaces and plastic flow rules. The evolution of the hardening modulus is guided by means of uniaxial cyclic laws.[7]

The proposed model, which belongs to the first category, extends the earlier degradation rule[5,6] for the unloading stiffness before yielding. Therefore, permanent strains reflect a more realistic behaviour of RC cracked members and at the same time, a uniform evolution of stiffness up to failure is assured. The pinched shape associated with diagonal shear cracks is modelled by means of the previous parameter proposed by Roufaiel and Meyer[6] based on the strong correlation found between the degree of pinching and the relative magnitude of shear at the section.[11] Additionally, the strength reduction, stiffness degradation and energy dissipation are directly dependent on the load level and the cyclic loading, which are described with a minimized number of state variables represented by a new cyclic parameter. These characteristics are outlined in the present paper where the principal assumptions made are:

1. small deformations of beam elements compared to the beam length,
2. kinematic field based on the Euler–Bernoulli hypothesis,
3. axial force and torsional moment depend linearly on axial elongation and angular displacement,
4. implicit shear force induces an increase of flexion strain,
5. decoupled moment–curvature relationships with respect to the local bending axes of the beam element,
6. axial force evaluated from gravity conditions remains constant through all the step loads.

### 2.2. *Primary envelope curve*

The trilinear moment–curvature diagram characterizing the monotonic response of a reinforced concrete section (Figure 2) is defined by three critical strain conditions at cross-section level for each direction of flexion; i.e. cracking of concrete $(M_{cr}, \phi_{cr})$, yielding of tensile steel $(M_y, \phi_y)$ and the ultimate strain of compressed concrete $(M_u, \phi_u)$. These points are calculated on the assumption that plane sections remain plane even up to incipient failure and assuming that strain–stress relationships for concrete and steel are known. In addition to the assumption of plane sections, a perfect bond between concrete and steel is assumed.

Experimental tests show that RC sections exhibit considerable capacity for plastic curvature beyond the peak of the moment–curvature curve, which results in significant increase of strength and ductility of cross-sections due to confinement of steel hoops. Several models for the compressive strain–stress behaviour of concrete confined by rectangular hoops have shown that the principal phenomena that should be reflected are the enhanced ductility due to strain gradient and the dependence of concrete strength on the level of axial load.

The elastic and plastic behaviour of RC columns yielding in flexure has been studied by many researchers, where the ultimate curvature $\phi_u$ was defined when the compressive strain of concrete reaches 0·003 in ACI or

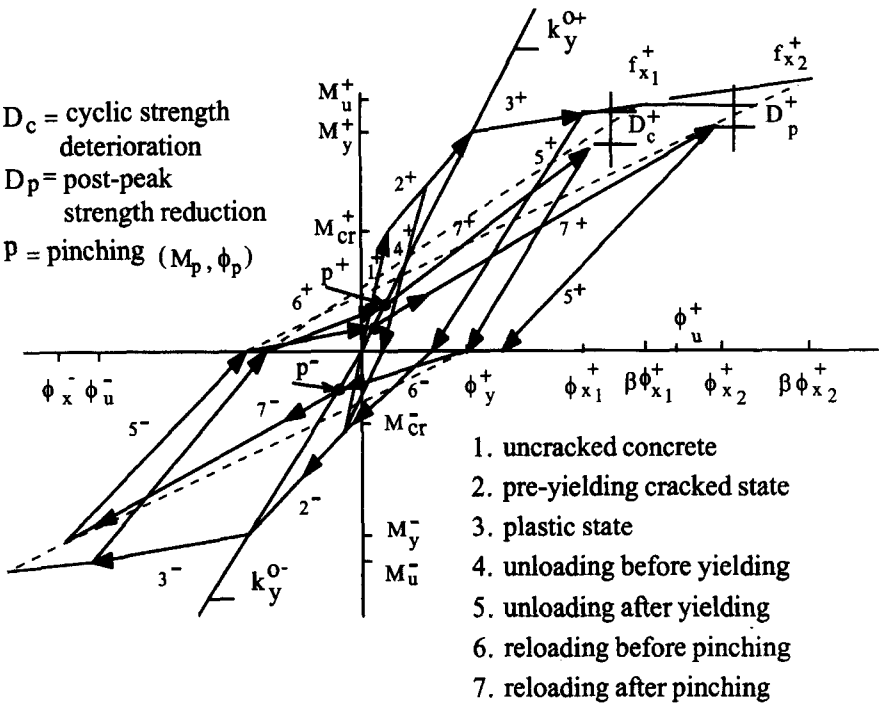


Figure 2. Hysteretic model

0·0035 in CEB. Experimental work carried out by Murakami and Imai[12] has shown that even to cyclic loads, moment capacity is not reduced at those limit strains. Similarly Shamin and Khoury[13] have found a crushing strain varied from 0·0045 to 0·0063 and a useful strain $\varepsilon_{max}$ varied between 0·025 and 0·042.

An analytical versus experimental comparison of moment–curvature relations for tied concrete columns subjected to axial load and flexure shows the effect of high axial loads on final crushing strain.[13] In order to take into account this effect, the same factor $\eta$ proposed by Shamin and Yeh[14] has been used. It should be noted that all strain–stress relationships for confined concrete of the reported analytical models have a greater concrete strength compared to Sheik and Uzumeri Model,[14] resulting in an overestimated capacity of sections and not only as an effect of axial load.

Two different levels of axial load with different lateral steel configuration are compared with the algorithm (Figure 3). In all models, the resistance drop-off is correlated to the shape of each concrete strain–stress relationship used. In this work the softening branch is managed as a part of the hysteretic rules. In fact, only the moment capacity corresponding to the predefined 'crushing' strain of concrete is needed. However, greater levels of strain were used to compare the response of the integration process, giving at the same time an additional criterion to redefine the ultimate strain of compressed concrete, taken here as the latest maximum strain before the first resistance reduction in the post-yielding phase.

### *2.3. Cracking/yielding behaviour*

Even before yielding, concrete structures exhibit a stiffness degradation. Experimental results give evidence of the occurrence of residual strains due to cracking before attaining the yielding point.[15] The assumption of neglected residual curvatures up to yielding is not able to describe correctly the dissipated energy and thus the hysteretic damping.[16] The non-linear simulation of concrete structures subjected to low load levels needs at least the identification of the cracking point.

In the present formulation, cracking of concrete gives a limit on the elastic linear behaviour and permanent strains due to unloading occur when this limit is exceeded. However, the unloading stiffness remains unchanged until a critical strain ($\phi_e$) is exceeded and the stiffness degradation takes place (Figure 4).

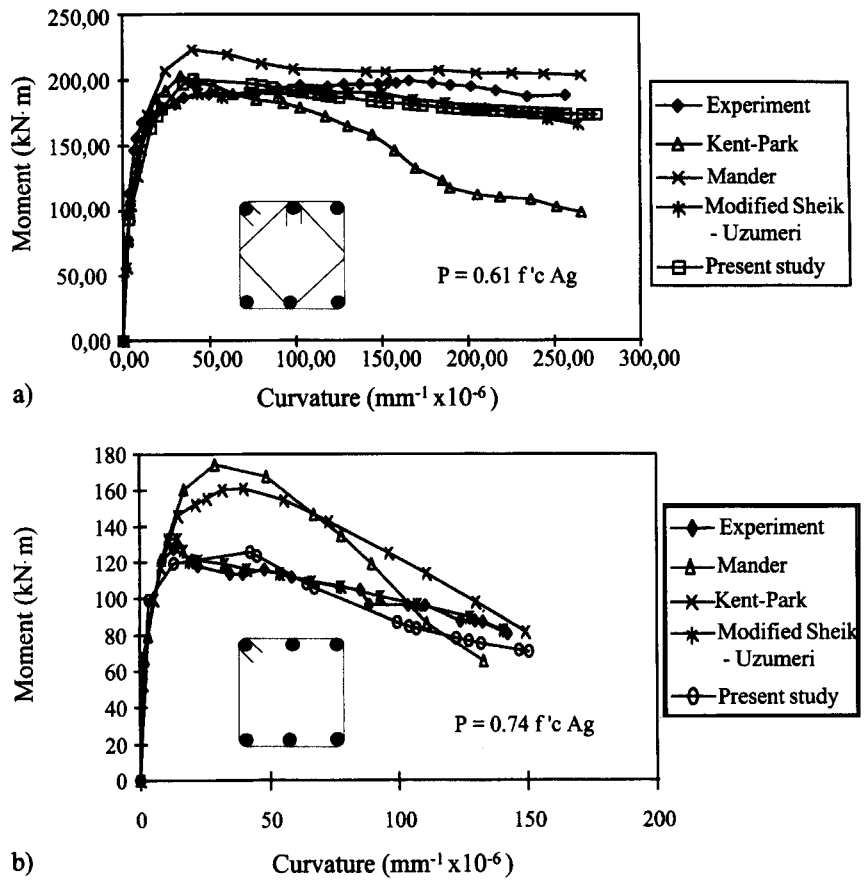


Figure 3. Different moment–curvature responses: (a) Comparison of experimental and analytical curves for specimen A-3[13], (b) comparison of experimental and analytical curves for specimen E-13[13]

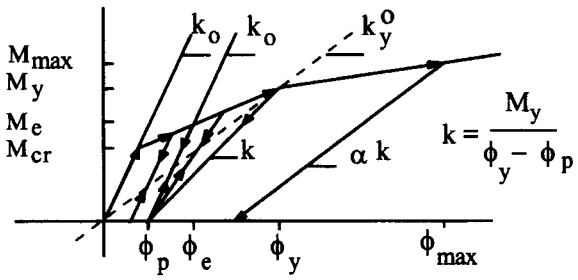


Figure 4. Unloading stiffness evolution

After yielding, the evolution of stiffness is defined by a damage parameter ($\alpha$) which is related to the maximum strain ever experienced and the yield strain ($\phi_y$):

$$\alpha = (\phi_y/\phi_{max})^{0.5} \quad (1)$$

This damage parameter used in several global models during the post-yielding behaviour[5,6,17] is adopted here, to provide continuity in the evolution of the stiffness degradation process. At the same time, the damage parameter defines also the minimum permanent strain ($\phi_p$), at yielding (Figure 4). The expressions for these

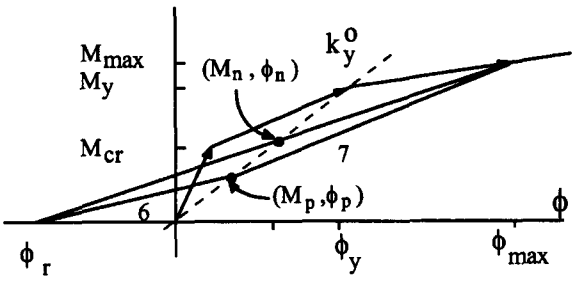


Figure 5. Pinching modelling

two limits are:

$$\phi_e = \phi_y / R^2 \tag{2}$$

with

$$R = k_0 / k_y^0 \tag{3}$$

$$\phi_p = \phi_e - M_e / k_0 \tag{4}$$

and

$$k = M_y / (\phi_y - \phi_p) \tag{5}$$

where $\phi_e$ = limit of linear elastic unloading; $\phi_p$ = minimum residual strain; $R$ = stiffness ratio with $k_0$ = initial stiffness; $k_y^0$ = secant stiffness at yielding and $k$ = unloading stiffness at yielding. If a bilinear curve $(M, \phi)$ is used, $\phi_e = \phi_y$ and $\phi_p = 0$ and accordingly the Roufaiel–Meyer stiffness evolution is found.[6] It should be pointed out that such a behaviour is not able to describe the energy dissipation before yielding.

*2.4. Shear effect*

The action of shear forces at regions of plastic hinging produces diagonal tension cracks tending to spread the zone of steel yielding further along the member than the bending moment diagram implies. Thus, in general, theoretical plastic rotations calculated from the bending moment diagram and the moment–curvature relationships will underestimate the actual rotations. When a member is loaded cyclically, there are stages in the loading at which open flexural cracks may exist across the full depth of the member, reducing the capacity of the concrete to carry shear force. Due to simplified kinematic hypothesis, Bernoulli beam models are unable to describe explicitly the effect of shear and bond degradation. The global response is entirely related to the flexural behaviour of cross-sections, whereas real behaviour includes at least the flexion and distortion of beams and columns, the slipping of longitudinal bars, the warping of the section and the dowel effect. These modes of deformation coexist and the mechanisms that produce them are interdependent.[18] Timoshenko beam models can introduce shear deformation laws; however, these laws are not commonly used due to the lack of experimental data and specially due to the coupling between shear and bending.

A strong correlation between the degree of pinching and the relative magnitude of shear at the section under consideration has been found. For small shear forces, no pinching is observed.[19] On the other hand, severe shear forces induce an important deterioration of stiffness during crack closure which consequently leads to a pinched reloading curve.[11]

In agreement with the simplified kinematic hypothesis, it is assumed that the diagonal shear cracking produces an increase of the flexion strain. This effect is considered only if the previous maximum excursion exceeds the yield strain ($\phi_y$) and the shear span ratio ($L/h$) is less than four. For instance, for reversal load a bilinear curve appears (lines 6 and 7 in Figure 2) and pinching is defined by a focal point $(M_p, \phi_p)$. $M_p = \alpha_p M_n$ and $\phi_p = \alpha_p \phi_n$, with $(M_n, \phi_n)$ corresponding to the intersection of the line defined by the points $(0, \phi_r)$ and $(M_{max}, \phi_{max})$ and the secant stiffness at yielding, $k_y^0 = M_y / \phi_y$. $\phi_r$ is the previous intersection with the strain axis and $\alpha_p$ is evaluated between 0 and 1 depending on the shear span ratio (Figure 5). Expressions for

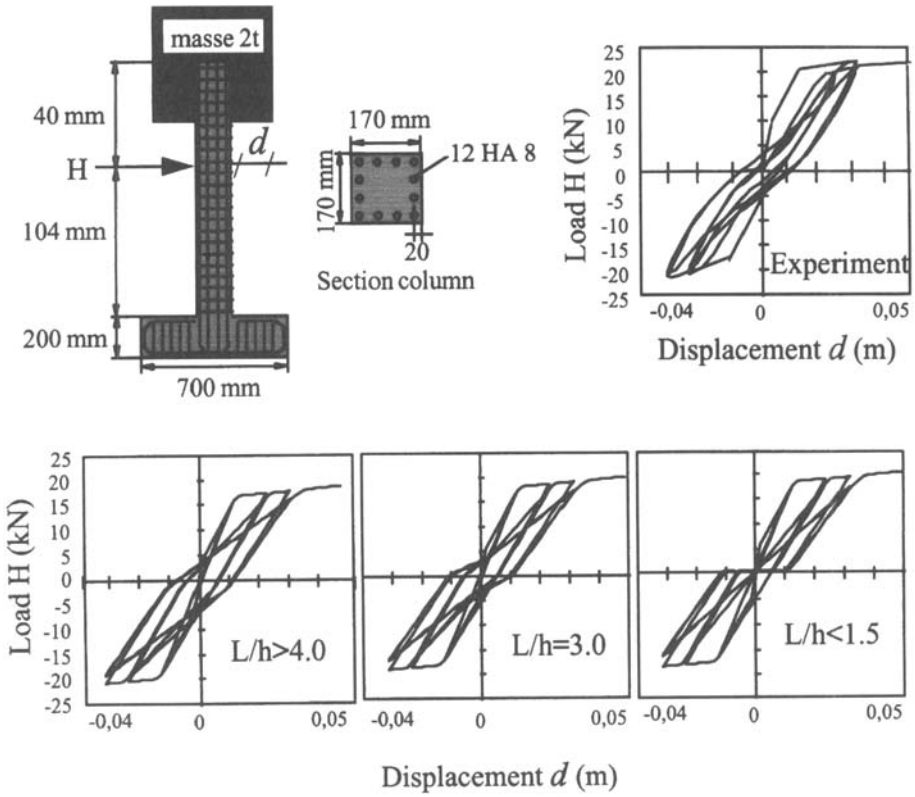


Figure 6. Induced pinching of hysteretic loops

$\alpha_p$ are taken from Reference 6. Experimental results[20] show that a deficient anchorage or degraded bond interface increases the flexion strains even in slender members. In the present model, if a pinched behaviour for slender members is expected, a fictitious shear span ratio can be introduced (Figure 6).

### *2.5. Strength deterioration*

Experimental results of RC members under repeated cyclic loading have shown the occurrence of strength degradation associated with cracking and bond deterioration at the steel–concrete interface. A correlation between damage index and strength deterioration has been widely used in several global formulations.[21]

The earliest references to damage are ductility based, arising from considerations of monotonic loading and low cycle fatigue.[22] Several variations include the modified flexural damage ratio of Roufaiel and Meyer.[6] Recently, ductility and energy dissipation have been considered in damage assessment.[23]

Roufaiel and Meyer[6] have proposed a damage indicator which relates the secant stiffness $(M_y/\phi_y)$, the ultimate secant stiffness $(M_u/\phi_u)$ and the secant stiffness at point of maximum strain ever experienced $(\phi_x)$, in the corresponding direction $(M_x/\phi_x)$:

$$D = \frac{(M_x/\phi_x) - (M_y/\phi_y)}{(M_u/\phi_u) - (M_y/\phi_y)} \tag{6}$$

where $\phi_y \leqslant \phi_x \leqslant \phi_u$ and $0 \leqslant D \leqslant 1$.

Garstka[24] and Sadeghi[25] have defined a damage parameter that takes into account the energy absorbed by the section through the cyclic loading. Empirical expressions have been proposed by Kunnath *et al.*[23] and Carr and Tabuchi[26] based on an energy criterion and deduced from cyclic tests.

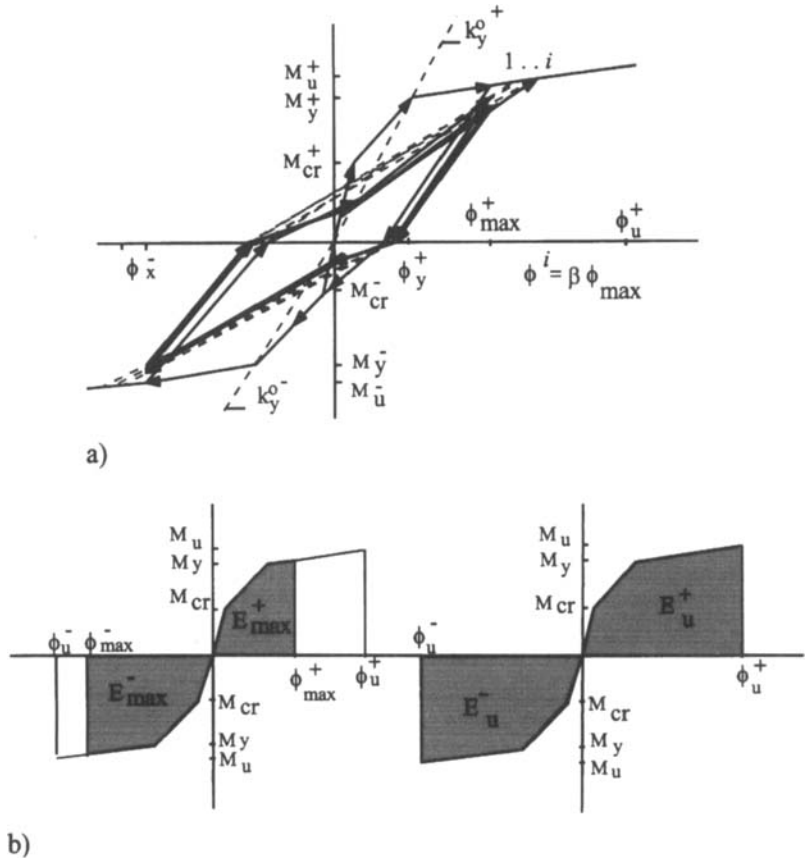


Figure 7. Strength deterioration at cross-section level: (a) Focal point evolution $i$ before the critical strain $\phi_u$, (b) total absorbed energies at maximum and ultimate strain

In order to take into account the strength deterioration in the cross-section due to cyclic loading, in both pre-peak strain range ($M_y \leqslant M_x \leqslant M_u$) and post-peak strain regime ($M_x > M_u$), a new cyclic parameter ($\beta$) is proposed. This parameter is used to define a focal point associated with a strain level ($\beta\phi_{max}$) and depends on a damage index ($D_{max}$), on an accommodating factor ($A_{max}$) and on the number of cycles ($n$), experienced up to the maximum strain level (Figure 7):

$$\beta = 1 + \sum_{i}^{n} [D_{max} A_{max}]^i$$

then

$$\beta = 1 + \sum_{i}^{n} \left[ \frac{E_{max}}{E_u} \frac{M_{max}\phi_{max}}{M_u \phi_u} \right]^i \tag{7}$$

where $E_{max}$ and $E_u$ are the total absorbed energy at the $\phi_{max}$ and $\phi_u$ strains respectively. Every time the maximum strain ($\phi_{max}$) ever experienced is updated, $i$ and $\beta$ are initialized to zero and one, respectively, while $D_{max}$ and $A_{max}$ remain constant throughout the cyclic loading.[27]

The value of $\beta$ becomes stable after four or five cycles at $\phi_y \leqslant \phi_{max} \leqslant 0{\cdot}5\phi_u$ with a reduction strength of about 5 per cent, whereas in the case of strain levels close to failure ($0{\cdot}9\phi_u \leqslant \phi_{max} \leqslant \phi_u$), the accommodation appears only after about twenty cycles with a strength reduction close to 40 per cent.

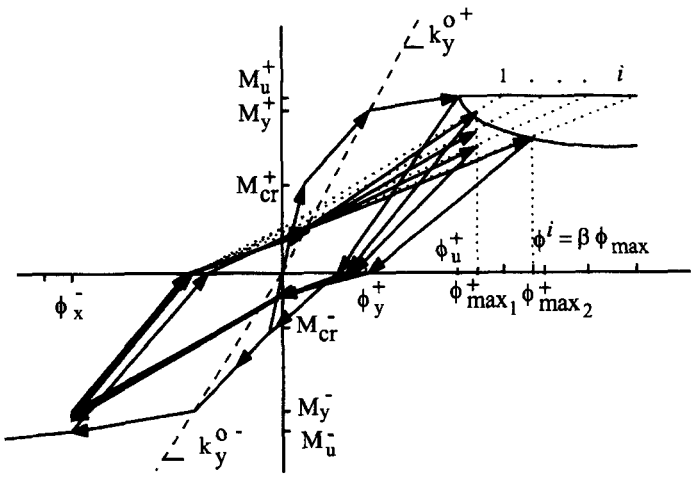


Figure 8. Focal point evolution $i$ after the critical strain $\phi_u$

*2.6. Softening behaviour*

It is generally accepted in the classical theories of limit analysis that an increase of the strain ($\phi_u$) occurs, without a decrease in moment capacity ($M_u$). In most of the cases, experimental results on the behaviour of RC beams under monotonic and cyclic loading show a descending branch in the force versus displacement curve after the peak of the moment–curvature diagram has occurred (characterizing the softening phenomenon of concrete in compression).

Several investigators have defined failure as the point where the member strength (moment) at maximum displacement (curvature) has dropped below 85 per cent of the initial yield strength ($M_y$). However, if the member is subsequently loaded beyond this maximum displacement or curvature, its moment can be observed to increase even more; consequently the failure moment and the corresponding curvature need to be redefined as it was pointed out at the beginning of this paper. A section may fail in flexure due to concrete crushing or fracture of the tensile steel. The magnitude of failure values are governed by longitudinal steel percentage and steel distribution, lateral confinement, and axial load.

The cyclic parameter $\beta$ previously defined allows to manage in the post-peak regime the envelope curve and the reduced strength ($M'_u$) of the cross-section at the same time (Figure 8). In this case $\beta$ is calculated putting $E_{max} = E_u$, $M_{max} = M'_u$ and $\phi_{max} = \phi'_u$. Accordingly $\beta = 1 + n$ (with $n \geqslant 1$) leads generally to a quick strength reduction of $M'_u$ throughout the cyclic load, accentuated by the importance of the strains ($\phi \gg \phi_u$).

*2.7. Hysteretic damping*

During seismic loading, acceleration ground motion shows a reduction intensity of amplitudes before the seismic excitation completely vanishes. Consequently, maximum displacements in both directions are no longer attained.

In the proposed model, the unloading branch before yielding remains parallel to unloading stiffness in agreement with the last maximum strain ever experienced. Consequently intersection with the horizontal axis produces a reduced residual strain. For reloading, the maximum strain ever experienced in the reverse direction stands as a focal point, which when associated to reduced residual strain gives a slightly increased reloading stiffness. As a result, the strain reached during the previous load cycle cannot be attained. At unloading the process is repeated and hysteretic loops progressively close, accompanied by decreasing strains.

After yielding, the focal point translates as a result of the deterioration rule and the number of applied load cycles which leads to a further decreasing of the unloading stiffness and residual strain. Once the deterioration rule stabilizes, the described behaviour before yielding is regained.

*2.8. Finite element implementation*

The dynamic equilibrium equations were implicitly integrated in time, by the Newmark trapezoidal rule algorithm implemented in CASTEM2000.[28] This is a general purpose computer code partially based on an object oriented type approach which offers a large set of tools for engineering use. The general equation of motion is given by

$$\mathbf{M}\ddot{x} + \mathbf{C}\dot{x} + \mathbf{K}x = F(t) - F_{\text{int}} \tag{8}$$

In the elastic case, the mass matrix **M** and the stiffness matrix **K** are calculated at the beginning of the computation. In the non-linear case, the mass matrix is constant and the equilibrium is achieved using the modified Newton–Raphson method, where $F(t)$ and $F_{\text{int}}$ are the time dependent load forces and the internal nodal forces accordingly. The stiffness matrix is evaluated from a finite two-nodes beam element with six degrees of freedom at each end node. The generalized strain field is calculated directly by compatibility conditions[1] from both end node displacement field $x$. The damping matrix **C**, proportional to the mass and the stiffness matrices ($\mathbf{C} = \alpha\mathbf{M} + \beta\mathbf{K}$) is assumed null in the present formulation.

## 3. NUMERICAL EXAMPLES

*3.1. Beam-column subassembly*

The model has been tested on isostatic and hyperstatic structural RC members subjected to monotonic, cyclic and dynamic loads. The numerical investigation presented here concerns in the first case, a beam-column subassembly subjected to reverse cyclic loading, tested by Del Toro Rivera.[15] The specimen considered is an interior joint of a frame with 4 m bays and 2 m storey heights. The geometric characteristics and the reinforced layout are described in Figure 9. Basic concrete parameters are $E_c = 37\,000$ MPa, $f'_c = 41$ Mpa, $f'_t = 4{\cdot}1$ Mpa, $\nu = 0{\cdot}2$ and steel parameters are $E_s = 200\,000$ MPa; yielding limit $f_y$ 490 MPa ($\phi$12), 440 MPa ($\phi$14), 550 MPa ($\phi$20). The boundary conditions are defined in such a way that the test can reproduce the response of a joint in a real building. First, a vertical prestressing load (200 kN) is applied to the column and an initial flexural load is introduced by loading vertically (22 kN) the beam ends. These loads simulate the dead weight of the building and the service loads acting on the floor. Beam and column members have been divided in finite elements of uniform length (0·5 m).

The vertical displacements of the beam ends are prevented and an alternating horizontal displacement is imposed on the base of the column simulating the seismic action. The loading consists of a series of cycles of increasing amplitudes; a set of five cycles is carried out in order to check the stability of the structural properties under repeated loading.

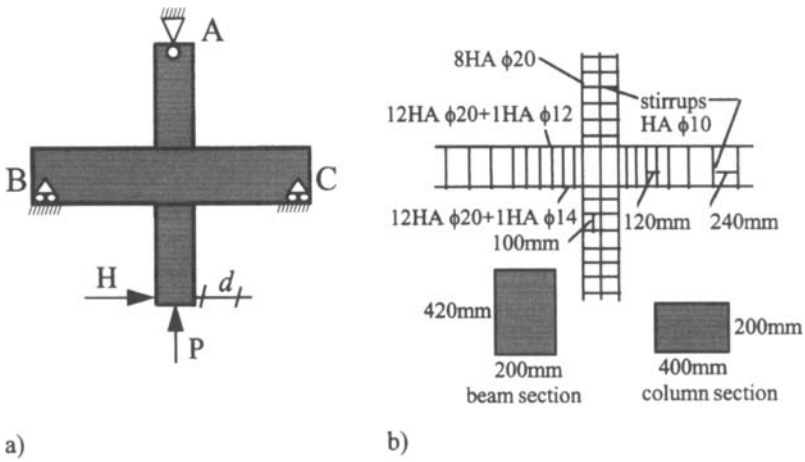


Figure 9. Interior beam-column joint of a RC frame: (a) Boundary conditions, (b) reinforced layout

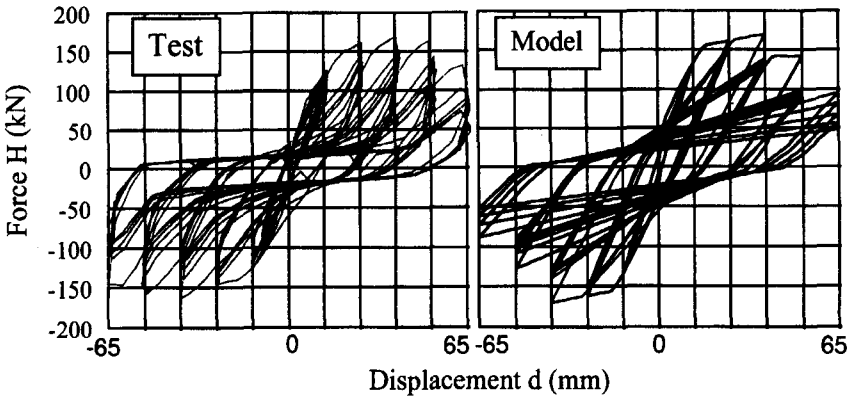


Figure 10. Experimental and numerical cyclic response

Table I. Residual strains and strength deterioration at different cycle levels

| Cyclic displacement (mm) | Residual deformation (mm) | | Strength reduction (%) | |
|---|---|---|---|---|
| | Measured | Calculated | Measured | Calculated |
| 26 | 10·21 | 7·69 | 12·5 | 7·4 |
| 39 | 22·29 | 17·71 | 27·0 | 23·7 |
| 52 | 33·43 | 29·70 | 37·6 | 42·9 |
| 65 | 46·42 | 42·71 | 43·0 | 44·4 |

The first set of cycles has an amplitude of $d = 10$ mm and represents a service load. The following cycles ($d = 13, 26, 39$ mm) bring the structure into the post-elastic domain, and the last cycles ($d = 52, 65$ mm) make the structure experience a softening branch.

The global response of the subassembly concerns the history of the horizontal displacement $d$ at the base of the column, versus the horizontal load $H$. The numerical predictions for a set of five cycles at each deformation level are compared with the experimental results. Figure 10 shows good agreement in the evolution of the stiffness degradation and of the permanent deformations. A better estimation of residual strain can be observed at high load levels (Table I). The calculated strength reduction between the maximum strength at first and last load cycle for each imposed displacement, agrees also well with the experimental results; however, the observed cyclic deterioration before the softening branch is more accentuated in the test than that observed in the model. On the other hand, calculated strength deterioration is slightly greater at failure limits.

Stiffness degradation, permanent deformations and energy dissipation agree quite well with the observed results. However, the pinching of the hysteresis loops is not described. In fact, for the proposed model, the shear span ratio of beams are greater than four and on the other hand, the shear span ratio of columns is approximately equal to 2·6. Nevertheless, for this range of displacements the columns remain below the yield point. Furthermore, Bernoulli beam models are unable to describe the effect of shear and bond degradation within the joint. Indeed, with this approach the joint behaves as a rigid block (conservation of the right angles between beams and columns) and the global response is entirely related to the flexural behaviour of cross-sections in the joint neighbourhood.[29]

### *3.2. Column subjected to dynamic loading*

The second application concerns a column subjected to dynamic loading tested by Gauvin[20] on the shaking table at Saclay, France. Geometric characteristics and test set-up are shown in Figure 11.

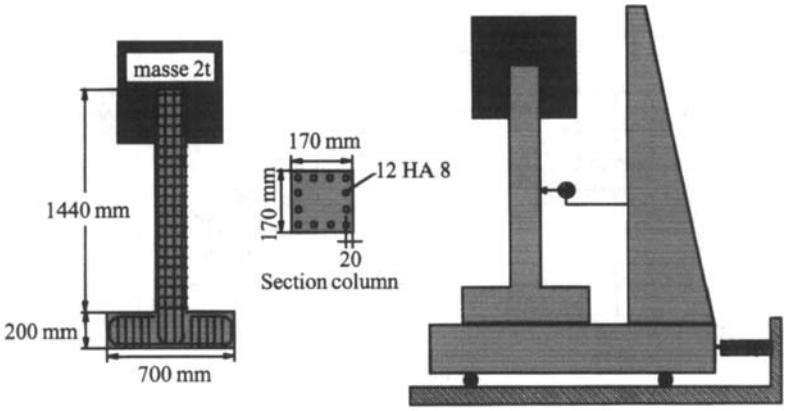


Figure 11. Dynamic column test: geometric characteristics and set-up

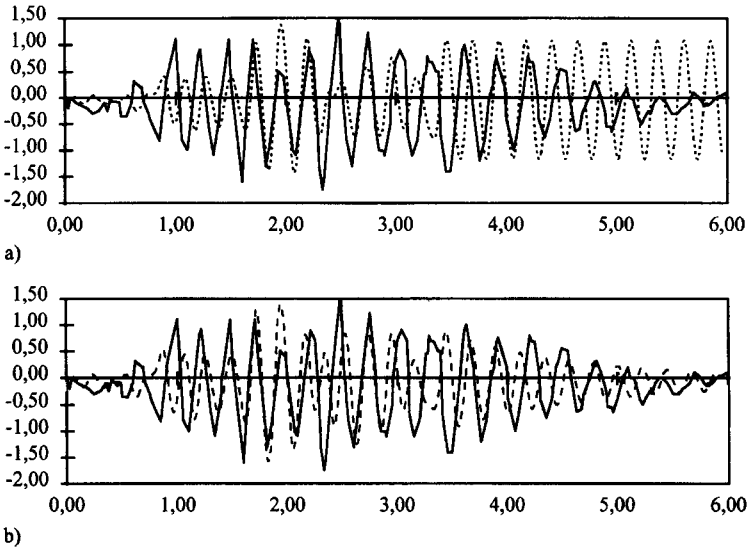


Figure 12. Test 1—displacement (mm) versus time (s) at mid-height: (a) Acceleration = 1·9 m/s$^2$ (———) test, (– – –) null strain at yielding; (b) acceleration = 1·9 m/s$^2$ (———) test, (– – –) proposed model

Basic concrete parameters are $f'_c = 42$ Mpa, $\varepsilon'_c = 0{\cdot}0018$, $E_c = 33\,000$ Mpa and steel parameters are $f_y = 445$ Mpa, $f_u = 540$ Mpa, with ultimate strain $\varepsilon_u = 9$ per cent. The column is subjected to a series of earthquakes of increasing amplitude lasting about 3·5 s. Here only the first three runs corresponding to a maximum base acceleration of 1·9, 4·1 and 5·2 m/s$^2$ are compared with numerical predictions.

The first run is also compared with a preceding model[16] assuming zero permanent strains up to yielding. At that level of strain, it is not possible to describe with such assumption the hysteretic dissipation when seismic excitation decreases (Figure 12(a)). In contrast, permanent strains due to cracking, reveal a more realistic behaviour in terms of energy dissipation (Figure 12(b)).

In the second run (Figure 13(a)), the differences at the top of the column are not greater than 12 per cent and the hysteretic damping after the dynamic excitation is well estimated. For the third run (Figure 13(b)), there is better correlation between maximum amplitudes at a given time-step. Furthermore, good agreement is observed between the frequencies of the experimental and analytical response. The calculated displacements at the top of the column are close to experimental data and the difference is of the order of 10 per cent

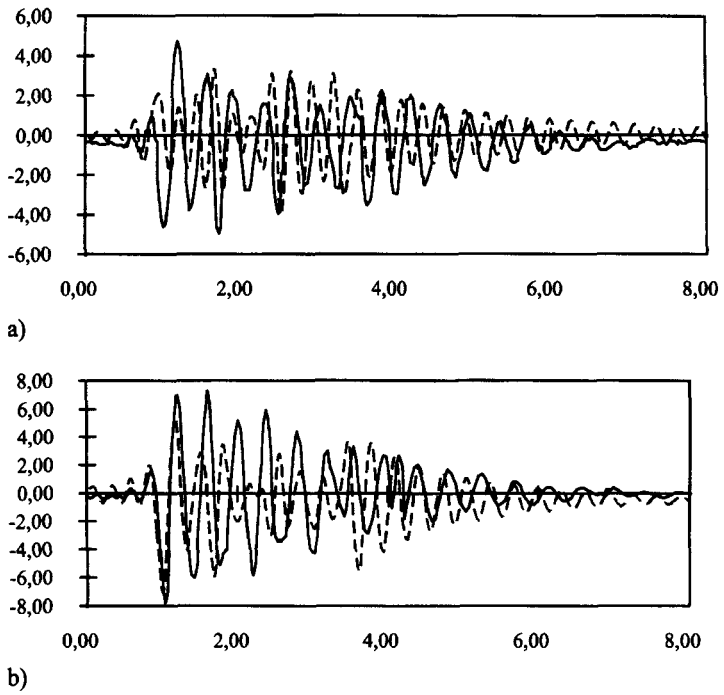


Figure 13. Subsequent dynamic loading: (a) Acceleration = 4·1 m/s² (———) test, (– – –) proposed model; (b) acceleration = 5·2 m/s² (———) test, (– – –) proposed model

Table II. Numerical and experimental maxima displacements and frequencies

| | Mid-height $d$ (mm) | | Top $d$ (mm) | |
|---|---|---|---|---|
| Run | Calculated | Test result | Calculated | Test result |
| 1 | 1·46 | 1·75 | 4·30 | 4·46 |
| 2 | 3·98 | 4·99 | 11·70 | 13·25 |
| 3 | 7·09 | 7·78 | 19·20 | 21·46 |

| Run | Calculated frequency (Hz) | Measured frequency (Hz) |
|---|---|---|
| 1 | 4·17 | 3·67 |
| 2 | 3·60 | 2·80 |
| 3 | 3·00 | 2·50 |

(Table II). This shows the ability of the model to describe a correct increase of the structural damage accordingly with subsequent inelastic excursions.

### *3.3. Four storey RC full scale frame*

An RC frame was used as a validation of a complete structure. An experimental test on a four storey full-scale RC frame was carried out in the European Laboratory for Structural Assessment at Ispra Joint Research Center in Italy. The structure has plan dimensions of 10 m × 10 m measured from column axis. Inter-storey heights are 3·5 m for ground storey and 3 m for subsequent storeys. The structure is symmetric in

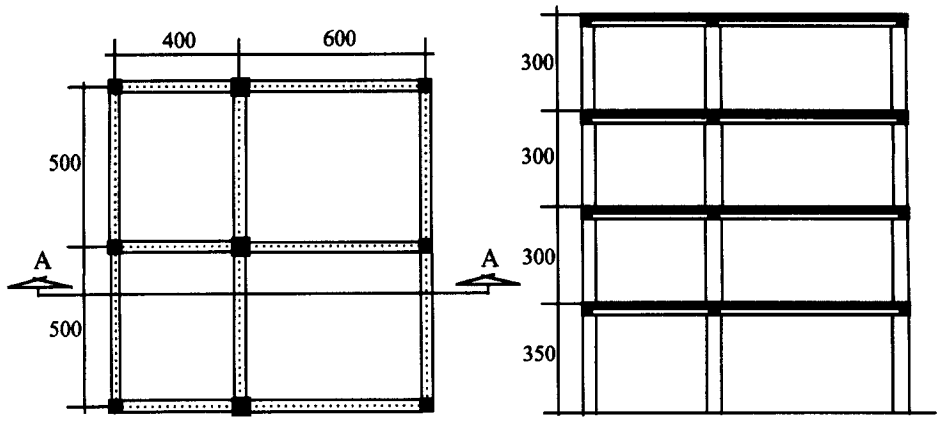


Figure 14. Four storey full scale RC frame

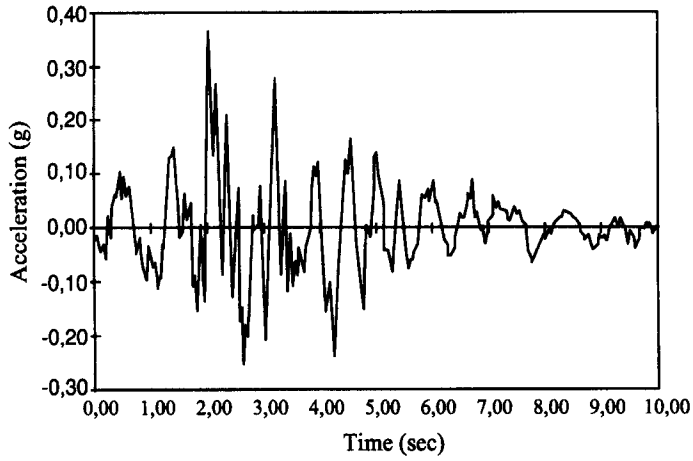


Figure 15. Friuli-like generated accelerogram S7

direction of testing with two equal spans of 5 m, whilst in the other direction it is slightly irregular with 6 m × 4 m span lengths (Figure 14). All columns have square cross-sections with 0·4 m side for exterior columns and 0·45 m for the interior column. All beams have rectangular cross-section with total height of 0·45 m and width of 3 m. A solid slab with thickness of 0·15 m has been adopted for all storeys.

Assumed typical design loads correspond to additional dead load 2 kN/m$^2$ to represent floor finishing and partitions, and live load 2 kN/m$^2$, with a high seismicity peak ground acceleration 0·3 g, soil type B and importance factor equal to one. All members were detailed in accordance with Eurocode-8 rules (EC-8). Details of reinforcement layout are reported in Reference 30. In all columns, axial forces were lower than the upper limit given in EC-8, and the beam–column joints turned out to be able to resist the shear forces by means of concrete struts.

In order to define the experimental program, a set of artificial accelerograms were generated by using the waveforms derived from a real signal[31] with a total duration of 10 s. The amplitude of the signal to be used was fixed at 1·5 times the amplitude of the reference signal, corresponding to a peak nominal base acceleration equal to $1{\cdot}5 \times 0{\cdot}3 = 0{\cdot}45\ g$ (Figure 15). Torsional effects are not present in the global behaviour of the structure. In fact, equal storey displacements are applied at external frames. Due to slab stiffness,

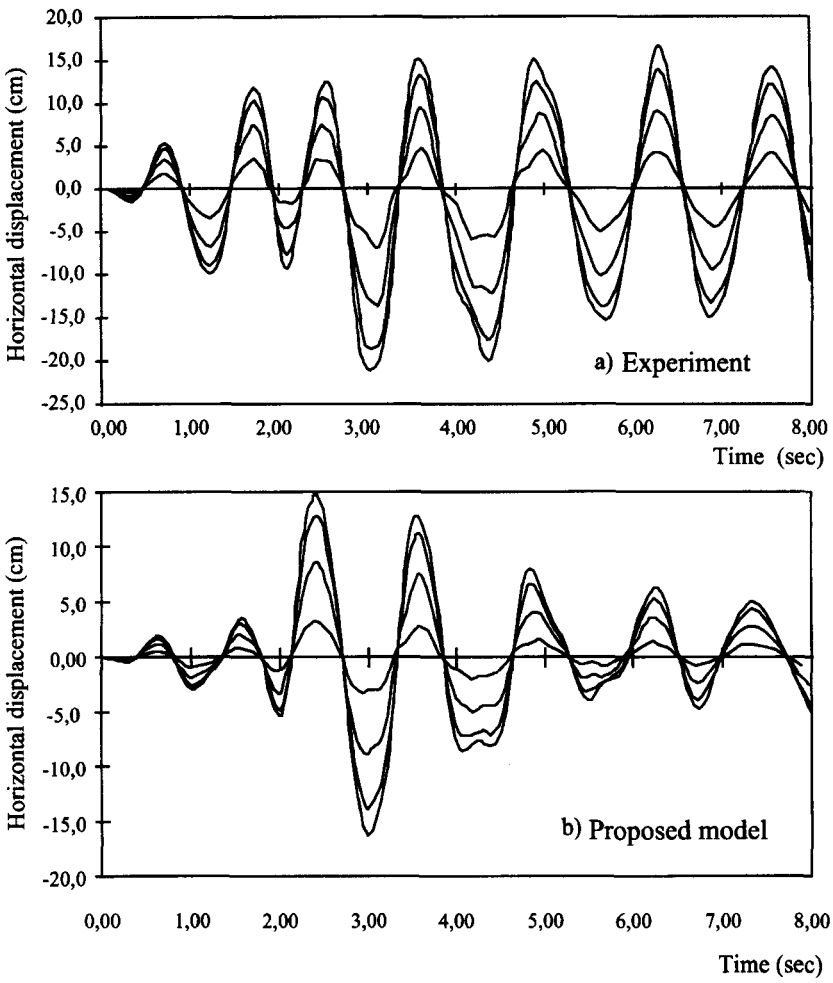


Figure 16. Time history of storey displacements: (a) Experiment, (b) proposed model

almost the same lateral displacement of interior frame can be expected. Taking into account this behaviour only the interior frame has been modelled with 5 m of slab width.

The complete time history of storey displacements are compared in Figure 16. A difference of 16·9 per cent of top displacement is found by the proposed model. The fundamental frequency of experimental and numerical response are calculated by the resulting transfer function of the spectral Fourier analysis. The difference with the experimental frequency is 9·4 per cent. Frequency evolution and base shear force predicted by the present analysis show a greater structural stiffness with respect to observed values. In fact, initial conditions introduced for the global model (i.e. lateral stiffness) were greater than that measured before the test. In reality, ISPRA structure[30] was built outside the laboratory test set-up. Transportation to the test place introduced a slight unevaluated damage. However, in the analysis performed by the proposed model, all uncracked concrete modulus were considered. This means that stiffness degradation and strength reduction evolution increase significantly after cracking. Initial damage would produce analytical displacements and frequencies closer to experiment results. Nevertheless, initial damage was deliberately not introduced in order to perform a predictive analysis.

The experimental time history of top displacement is compared with the experimental response of the proposed model and the modified Takeda-based model performed by Fardis and Panagiotakos[32] (Figure 17). In this last one, the used bilinear skeleton curve was determined assuming linear behaviour of

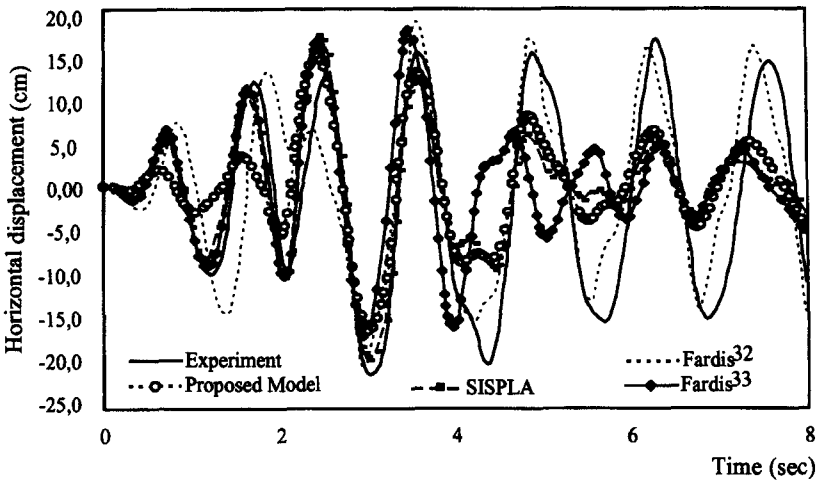


Figure 17. Experimental versus analytical comparison of top storey displacement

Table III. Experimental versus numerical global response comparison

| | Experiment | Proposed model | ANSR-I[32] | SISPLA[33] |
|---|---|---|---|---|
| $d_{max}$/time step | 21·0/3·02 | 17·45/3·0 | 20·02/2·95 | 19·6/3·0 |
| Averaged frequency | 0·820 | 0·905 | 0·782 | 1·05 |
| Base shear (kN) | 1440 | 1490 | 1296 | 1429·6 |

concrete in compression and a constant value of axial forces (zero in the beams). The two hysteresis parameters characterizing the degradation of unloading stiffness and the point of reloading branch were adjusted so that the corresponding hysteretic energy agrees well with experimental results. Viscous damping was taken as a combination of mass-proportional and stiffness-proportional, with proportionality factors chosen so that damping was 5 per cent of critical at $T = 1{\cdot}2$ s and $T = 0{\cdot}8$ s for a cracked elastic structure for which the periods are about twice those of the uncracked structure. The response described by the modified Takeda model has needed a previous identification of behavioural parameters adjusted by the test results. An earlier prediction[33] assuming current damage parameters and damping coefficients is shown in the same Figure 17.

The same structure was analysed by Coelho and Carvalho[33] based on the computer program SISPLA where beams and columns were idealized as linear elements with inelastic flexural springs at the ends and assuming elastic behaviour in the remaining portion of each element. The constitutive relations of the inelastic springs were defined by the moment–curvature diagrams using an hysteretic Takeda-type model including stiffness degradation. The initial elastic branches of those diagrams were taken considering cracked cross-sections. The coefficients affecting mass and stiffness matrices were evaluated in order to achieve a damping ratio of 2 per cent in the first and the third vibration modes. The time history of top displacement of the refined[33] analysis is shown in Figure 17. Maximum amplitudes, maximum base shear and fundamental frequencies are compared in Table III.

It is interesting to notice that even when seismic excitation decreases (after 4 s), the top displacement in the positive direction remains important. All the numerical responses reported in Reference 33 show a reduction of amplitudes due mainly to the non-linear behaviour of materials. In general, between 0 and 4 s the

dispersion of the predicted response decreases as the intensity of the seismic excitation increases. That means that the more the non-linear response becomes relevant the less important are the assumptions made in what concerns the initial stiffness and the behaviour is controlled by the non-linear description of the structural members.

## 4. CONCLUSIONS

The non-linear behaviour of RC structures involves material non-linearities, structural geometry and load histories. A simplified hypothesis based on mechanical concepts, observed experimental results and the degree of desired information deal with three usual modelling scales. Between these levels of analysis, global approaches have a wide margin of applicability for structures composed of beams and columns.

In this work, an accurate limit analysis of the envelope curve defines correctly the occurrence of hardening and softening behaviour. The strength and stiffness degradation in the hardening and the softening branches as well as the hysteretic damping have been described with the aid of a new parameter based on energy criteria and phenomenological considerations. The major benefit of the present formulation resides on the continuous and load depending evolution of this parameter and hence on the reduced parameters involved into the problem definition. The load dependence of the degradation and dissipation process characterized by this parameter is demonstrated by three examples with a major description of the degradation process per cycle in the first one. In addition to several earlier models, the present formulation describes the energy dissipation before yielding preserving a continuous evolution of the damage process up to failure. The advantages of such a behaviour is demonstrated in the second example. In the third example, the global response comparison with two Takeda-type models with classical degradation parameters and damping matrix, shows the role played by the proposed model during predictive analysis.

The proposed model takes into account the essential phenomena associated with the cyclic behaviour of RC members when variation in axial force can be neglected and flexion behaviour is predominant. Special cases, such as degraded bond interface and beam-column joint behaviour, are partially modelled. Most of the existing phenomenological models are based on uniaxial laws assuming a decoupled effect of normal force, shear and flexion. The plasticity-based approaches are the most appropriate to account for the interaction of internal forces. Consequently, a plasticity-based approach in generalized variables[34] will take advantage of the proposed uniaxial model to describe the evolution of a kinematic hardening parameter with regard to the interaction of axial force and flexion.

## REFERENCES

1. O. C. Zienkiewicz and R. L. Taylor, *The Finite Element Method*, 4th edn, McGraw Hill, London, 1989.
2. K. J. Mork, 'Response analysis of reinforced concrete structures under seismic excitation', *Earthquake eng. struct. dyn.* **23**, 33–48 (1994).
3. F. Taucer, E. Spacone and T. C. Filippou, 'Fiber beam-column element for seismic response analysis of reinforced concrete structures', *Report No. UCB/EERC-91/17*, Earthquake Engineering Research Center, University of California, Berkeley, CA, 1991.
4. B. A. Izzuddin, C. G. Karayannis and A. S. Elnashai, 'Advanced nonlinear formulation for reinforced concrete beam-columns', *J. struct. eng. ASCE* **120**, 2913–2934 (1994).
5. T. Takeda, M. A. Sozen and N. Nielsen, 'Reinforced concrete response to simulated earthquakes', *J. struct. div. ASCE* **96**, 2557–2573 (1970).
6. M. S. L. Roufaiel and C. Meyer, 'Analytical modelling of hysteretic behaviour of R/C frames', *J. struct. eng. ASCE* **113**, 429–444 (1987).
7. P. F. S. Chen and G. H. Powell, 'Generalized plastic hinge concepts for 3D beam-column elements', *Report No. UCB/EERC-82/20*, Earthquake Engineering Research Center, College of Engineering, University of California, Berkeley, CA, 1982.
8. M. Z. Cohn and W. Krzywiecki, 'Nonlinear analysis system for concrete structures: STRUPL-1C', *Eng. struct.* **9**, 104–123 (1987).
9. M. Sfakianakis and M. N. Fardis, 'Bounding surface model for cyclic biaxial bending of RC sections', *J. eng. mech. ASCE* **117**, 2748–2769 (1991).
10. J. L. Fléjou, 'Dynamic behaviour of civil engineering structures with semi-rigid joints' (in French), *Ph.D. Thesis*, Université Paris VI, France, 1993.
11. E. P. Popov, V. V. Bertero and H. Krawinkler, 'Cyclic behaviour of three R. C. flexural members with high shear'. *Report No. EERC* 72-5, Earthquake Engrg. Research Center University of California, Berkeley, CA, 1972.
12. M. Murakami and H. Imai, 'A study on influence of different loading histories on failure behaviour of RC columns yielding in flexure', *Trans. Japan concrete institute* **8**, 367–380 (1986).
13. A. S. Shamin and S. S. Khoury, 'Confined concrete columns with stubs', *ACI struct. j.* **90**, 414–431 (1993).

14. A. S. Shamin and C. C. Yeh, 'Analytical moment–curvature relations for tied concrete columns', *J. struct. eng. ASCE* **118**, 529–544 (1991).
15. R. Del Toro Rivera, 'Behaviour of RC beam-column subassemblies under alternating loading' (in French), *Ph.D. Thesis*, Ecole Nationale des Ponts et Chaussées, Paris, France, 1988.
16. D. Miramontes, O. Merabet and J. M. Reynouard, 'Hysteretic global model for the seismic analysis of RC structures' (in French), in *Proc. 7th Canadian conf. on earthquake eng.*, Montréal, Canada, 1995, pp. 253–260.
17. M. Saiidi and M. A. Sozen, 'Simple nonlinear seismic analysis of R/C structures', *J. struct. div. ASCE* **107**, 937–952 (1981).
18. F. Fleury, O. Merabet and J. M. Reynouard, 'Finite element analysis of reinforced concrete structures under seismic loading: modelling of the beam-column joint', in A. S. Elnashai (ed.), *5th SECED int. conf. on European seismic design practice, research and application*, Chester, U.K., Thomas Telford Services Ltd., London, 1995, pp. 395–402.
19. M. P. Chronopoulos and E. Vintzileou, 'Confinement of RC columns', in A. S. Elnashai (ed.), *5th SECED int. conf. on European seismic design practice, research and application*, Chester, U.K., Thomas Telford Services Ltd., London, 1995, pp. 341–348.
20. J. Gauvin, C. Jeandidier, J. C. Gauvert, J. C. Queval and H. Vaghi, 'Seismic tests of RC columns'. *Technical Report C.E.A.-D.M.T./78/177*, Saclay, France, 1978.
21. Y. S. Chung, C. Meyer and S. Massanobu, 'Modeling of concrete damage', *ACI struct. j.* **86**, 259–271 (1989).
22. Y. J. Park and A. H. S. Ang, 'Mechanistic seismic damage model for reinforced concrete', *J. struct. eng. ASCE* **111**, 722–739 (1985).
23. S. K. Kunnath, A. M. Reinhorn and Y. J. Park, 'Analytical modelling of inelastic seismic response of R/C structures', *J. struct. eng. ASCE* **116**, 996–1017 (1990).
24. B. Garstka, 'Investigations on resistance and damage behaviour of reinforced concrete linear elements considering shear effects under cyclic nonlinear loading', *Mitteilung Nr. 93-2*, Institut für konstruktiven ingenieurbau, Ruhr-Universität Bochum, 1993.
25. K. Sadeghi, 'Numerical simulation of RC column behaviour subjected to alternating deviated shear' (in French), *Ph.D. Thesis*, Ecole Centrale de Nantes, France, 1995.
26. A. J. Carr and M. Tabuchi, 'The structural ductility and damage index for reinforced concrete structures under seismic excitations', in T. Moan *et al.* (eds), *Proc. European conf. on structural dynamics—EURODYN '93*, Trondheim, Norway, Balkema, Rotterdam, 1993, pp. 169–176.
27. D. Miramontes, O. Merabet and J. M. Reynouard, 'Hysteretic beam model for the seismic analysis of RC structures', in A. S. Elnashai (ed) *5th SECED int. conf. on European seismic design practice, research and application*, Chester, U.K., Thomas Telford Services Ltd., London, 1995, pp. 403–410.
28. CEA, Commissariat of Atomic Energy, *CASTEM2000-User's Guide*, CEA Saclay, France, 1990.
29. F. Fleury, O. Merabet and J. M. Reynouard, 'A finite element for bond: Application to R/C beam-column joints subjected to cyclic reversed loads', in S. A. Savidis (ed), *Proc. 2nd. int. conf. on earthquake resistant construction and design*, Berlin, A. A. Balkema, Rotterdam, 1994, pp. 741–748.
30. P. Negro, G. Verzeletti, G. E. Magonette and A. V. Pinto, 'Test on a four-storey full scale R/C frame designed according to Eurocodes 8 and 2', *Preliminary Report EUR15879 EN*, European Commission, Joint Research Center, Ispra (VA), Italy, 1994.
31. A. V. Pinto and P. Pegon, 'Numerical representation of seismic input motion', in J. Donea and P. M. Jones (eds), *Experimental and Numerical Methods in Earthquake Engineering*, Kluwer, Dordrecht, The Netherlands, 1991.
32. M. N. Fardis and T. B. Panagiotakos, 'Earthquake response of RC structures', in A. S. Elnashai (ed), *5th SECED int. conf. on European seismic design practice, research and application*, Chester, U.K., Thomas Telford Services Ltd., London, 1995, pp. 11–18.
33. E. C. Carvalho (ed), 'Cooperative research on the seismic response of the reinforced concrete structures', *Final Report No. 4504-91-10 ED ISP P*, Libson, LNEC, 1993.
34. D. Miramontes, O. Merabet and J. M. Reynouard, 'Kinematic hardening model based on general plasticity for RC frames', in *Proc. 11th world conf. on earthquake eng.*, Acapulco, Mex., Elsevier, Amsterdam, CD-Rom version, 1996.